ANL/NT/CP-100475

RECEIVED
MAY 05 2000
OSTI

ANALYTICAL ELECTRON MICROSCOPY STUDY OF RADIOACTIVE CERAMIC WASTE FORMS

by

T. P. O'Holleran, *W. Sinkler, T. L. Moschetti, S. G. Johnson, and K. M. Goff

Nuclear Technology Division
*Engineering Division
Argonne National Laboratory-West
P. O. Box 2528
Idaho Falls, ID 83403-2528

The submitted manuscript has been created by the University of Chicago as Operator of Argonne National Laboratory ("Argonne") under contract No. W-31-109-ENG-38 with the U.S. Department of Energy. The U.S. Government retains for itself, and others acting on its behalf, a paid-up nonexclusive, irrevocable worldwide license in said article to reproduce, prepare derivative works, distribute copies to the public, and perform publicly and display publicly, by or on behalf of the Government.

To be Presented
at the ANS Embedded Topical Meeting
on DOE Spent Fuel and Fissile Material
San Diego, CA

June 4-8, 2000

Work supported by the U.S. Department of Energy, Office of Nuclear Energy, Science and Technology, and the Office of Environmental Management, under contract W-31-109-Eng-38.

DISCLAIMER

This report was prepared as an account of work sponsored by an agency of the United States Government. Neither the United States Government nor any agency thereof, nor any of their employees, make any warranty, express or implied, or assumes any legal liability or responsibility for the accuracy, completeness, or usefulness of any information, apparatus, product, or process disclosed, or represents that its use would not infringe privately owned rights. Reference herein to any specific commercial product, process, or service by trade name, trademark, manufacturer, or otherwise does not necessarily constitute or imply its endorsement, recommendation, or favoring by the United States Government or any agency thereof. The views and opinions of authors expressed herein do not necessarily state or reflect those of the United States Government or any agency thereof.

DISCLAIMER

Portions of this document may be illegible in electronic image products. Images are produced from the best available original document.

ANALYTICAL ELECTRON MICROSCOPY STUDY OF RADIOACTIVE CERAMIC WASTE FORMS

T. P. O'Holleran, W. Sinkler, T. L. Moschetti, S. G. Johnson, K. M. Goff
Argonne National Laboratory-West
P.O. Box 2528
Idaho Falls, ID 83403
(208) 533-7430

ABSTRACT

A ceramic waste form has been developed to immobilize the halide high-level waste stream from electrometallurgical treatment of spent nuclear fuel. Analytical electron microscopy studies, using both scanning and transmission instruments, have been performed to characterize the microstructure of this material. The microstructure consists primarily of sodalite granules (containing the bulk of the halides) bonded together with glass. The results of these studies are discussed in detail. Insight into the waste form fabrication process developed as a result of these studies is also discussed.

I. INTRODUCTION

Argonne National Laboratory has developed a ceramic waste form (CWF) to immobilize the halide high-level waste (HLW) stream from electrometallurgical treatment of spent nuclear fuel in a glass-bonded ceramic waste form[1]. The HLW stream consists of spent electrolyte (LiCl - KCl eutectic), fission products, plutonium and other transuranics, and some sodium chloride (from bonding sodium in the spent fuel). The waste bearing salt is absorbed (or occluded) into a dried zeolite (Linde Type A, ($Na_{12}Al_{12}Si_{12}O_{48}$)) at 500° C. The waste form is produced by sealing a 3/1 mixture (by weight) of salt-occluded zeolite and glass powders in an evacuated cylindrical stainless steel can (type 304L), and consolidating the mixture in a hot isostatic press (HIP) at 850° C and 100 MPa. During the HIP step, the crystalline salt occluded zeolite is converted to sodalite ($Na_6Al_6Si_6O_{24}$• 2NaCl), which is bonded together by a glassy phase comprising about 25% of the waste form by volume. Development work is currently focused on process scale-up and operations with fully radioactive material. The first fully radioactive HIP cans were prepared using a sample of salt that had been used to treat 100 Experimental Breeder Reactor II (EBR II) driver fuel assemblies. The nominal salt composition is shown in Table 1.

Table 1. Assessed composition of 100-driver salt, batch # ERBF25C [Ref 1]. The sample is also expected to contain 350 μg/g I^- and 45 μg/g Br^-.

Element	wt %	at %
K	21.3	17.27
Li	5.87	26.82
U†	7.207	0.96
Na	1.9	2.62
Nd	0.7	0.15
Cs	0.66	0.16
Ce	0.42	0.09
Pu*	0.291	0.04
Ba	0.25	0.06
Pr	0.21	0.05
La	0.21	0.05
Sm	0.21	0.03
Sr	0.15	0.05
Y	0.12	0.04
Fe	0.066	0.04
Np	0.0265	<0.004
Cl††	57.63	51.55

† Isotopic composition approximately 60% ^{235}U, 40% ^{238}U

* Isotopic composition approximately 99% ^{239}Pu, rest ^{240}Pu and ^{238}Pu.

†† Calculated assuming anionic composition is 100% Cl^-, and standard chloride

stoichiometries for all elements (rare earths and actinides in trivalent state).

An understanding of the microstructure of the CWF is useful for interpreting results of waste form performance tests, and for developing models to predict long-term waste form behavior in a geologic repository. The microstructure of the CWF is typically characterized by a combination of scanning and transmission electron microscopy. When used in conjunction with X-ray spectroscopy and electron diffraction, these methods yield a detailed description of the CWF microstructure, ranging from relatively large-scale features such as grain size, phase distribution, and porosity, to small-scale details regarding interactions between glass and crystalline phases, and crystallography of finely dispersed nanocrystals. Microstructural characterization provides the technical basis for comparing results from tests on non-radioactive CWFs containing surrogates for fission products and actinides, and radioactive CWFs.

II. EXPERIMENTAL

A. Scanning Electron Microscope (SEM) Sample Preparation

Samples of ceramic waste form were removed from HIP cans by slicing the cans with a water-cooled diamond saw and core drilling the slices with a diamond core drill. The samples were mounted in epoxy mounts using a phenolic ring to confine the epoxy. The epoxy used to prepare the mount was Epofix® from Kodak, and was prepared according to the manufacturer's instructions. Tungsten powder (-325 mesh) was added to the epoxy to provide shielding during subsequent sample preparation and handling. After the epoxy had polymerized (approximately 24 hours), the samples were polished on a polishing wheel at 200 RPM using 180, 400, 600, 800, and 1200 grit silicon carbide paper in that order. Isocut® organic cutting fluid was used as a lubricant and to control dust. The initial coarse (180 grit) polish was necessary to remove epoxy that had at least partially covered the samples. After polishing and decontamination, the mounted samples were coated with approximately 280 Å of carbon in a Gatan ion beam coater.

B. SEM Description and Operating Conditions

A Zeiss DSM960A digital scanning electron microscope with a lanthanum hexaboride filament was used for this analysis. It is equipped with both secondary and back scattered electron detectors, as well as Oxford Instruments energy dispersive (EDS) and wavelength dispersive (WDS) X-ray spectrometers. The spectrometers are driven by Link ISIS Series 300 software, version 3.2. Winspec version 3.1 software is also available to drive the wave length dispersive spectrometer. The ISIS software also provides digital image acquisition, X-ray mapping, and line scan capabilities, and allows remote control of both the stage and electron beam.

The instrument was mostly operated at an accelerating voltage of 20 kV and an emission current of 15 μA with a 200 μm aperture in place, and at a working distance of 25 mm. Copper tape used to attach the sample mount to the microscope stage and provide electrical conductivity was also used to calibrate the energy dispersive spectrometer (EDS).

C. Transmission Electron Microscope (TEM) Sample Preparation

A sample of CWF for TEM was mechanically thinned and core drilled to produce a 3 mm disk of approximately 150 μm thickness. The disk was dimpled to a central thickness of approximately 20 mm, and was ion milled to perforation using 4 keV Ar^+ ions in a Gatan precision ion polishing system. Prior to examination, a 70 Å film of amorphous carbon was deposited on the sample in a Gatan ion beam coater.

D. TEM Description and Operating Conditions

TEM investigation used a JEOL 2010 TEM/STEM with lanthanum hexaboride filament and analytical pole piece. For chemical analysis, an Oxford Instruments ultra thin window energy dispersive spectrometer (EDS) was used.

III. RESULTS

The microstructures of all the 100-driver salt-loaded CWF samples were virtually identical, and closely resembled the microstructure of non-radioactive CWF materials made with surrogate fission products during process development. Backscattered electron (BSE) images representative of the overall CWF microstructure are shown in Fig. 1. The microstructure of the radioactive CWF (Fig. 1a) consists of granules of sodalite with glass between the granules, and bright white inclusions concentrated along the boundaries of the sodalite granules and at sodalite/glass interfaces. These high contrast inclusions usually contain rare earths and/or actinides, but are occasionally identified as halite (NaCl) inclusions. Within the sodalite granules, finer sodalite grains (several microns in diameter and hence not visible in Fig. 1) are sometimes observed surrounded by an intergranular glassy phase. This microstructure is very similar to that of CWF material fabricated with salt containing surrogate (non-radioactive) fission products (Fig. 1b). In the surrogate material, the bright white inclusions are fewer in number, and are usually identified as rare earth containing phases, or occasionally halite. Fig. 2 is a higher magnification SEM image showing several actinide bearing inclusions in a fully radioactive CWF material. Energy and wavelength dispersive X-ray spectroscopy showed that one of the inclusions (labeled P) contained both plutonium and uranium, while two others (labeled U) were found to contain only uranium. The predominance of uranium in the actinide inclusions is expected, since the salt used to fabricate this material contained 7.2 wt% uranium, but only 0.3 wt% plutonium. Portions of X-ray spectra from the inclusion labeled P in Fig. 2 are shown in Fig. 3. In addition to uranium, chlorine, yttrium, silicon, aluminum, sodium and oxygen are also identified in the EDS spectrum shown in Fig. 3a. The nature of the broad peak labeled K,U,Pu in Fig. 3a is revealed in the WDS spectrum shown in Fig. 3b, which clearly identifies plutonium. Some ambiguity is inherent in interpretation of X-ray spectra obtained from small features such as those shown in Fig. 2. Penetration and scattering of the incident electron beam below the surface of the sample activates a volume of material up to a depth of about 2 μm and out to a radius of about 1 μm that can contribute to the X-ray spectrum. Furthermore, when the SEM is configured for X-ray spectroscopy, clusters of nanocrystals in a matrix phase cannot be distinguished from solid inclusions because instrument conditions cannot be optimized for resolution. These considerations, along with

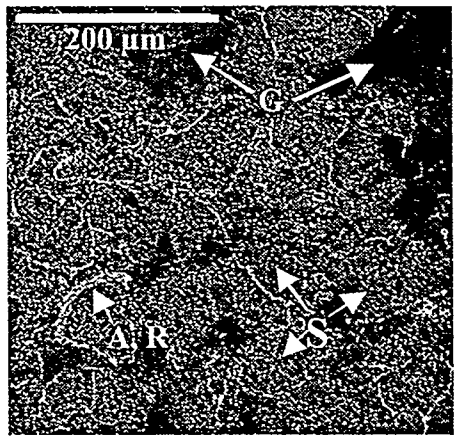

a.

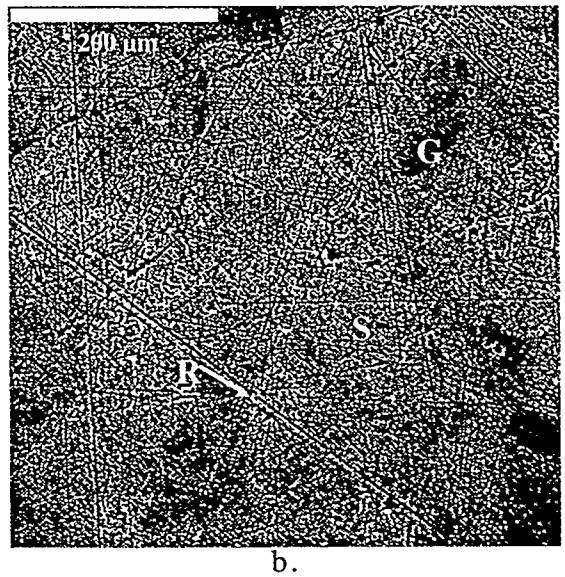

b.

Figure 1: Scanning electron micrographs obtained in back scattered electron mode (BSE) showing typical microstructural features observed in a. radioactive CWFs and b. non-radioactive CWFs (made with surrogate fission products): sodalite (S), glass (G), rare earth (R), and rare earth/actinide bearing phases (A, R). Much of the apparent porosity in a. is a sample preparation artifact resulting from modifications

to sample preparation procedures required to minimize personnel exposure.

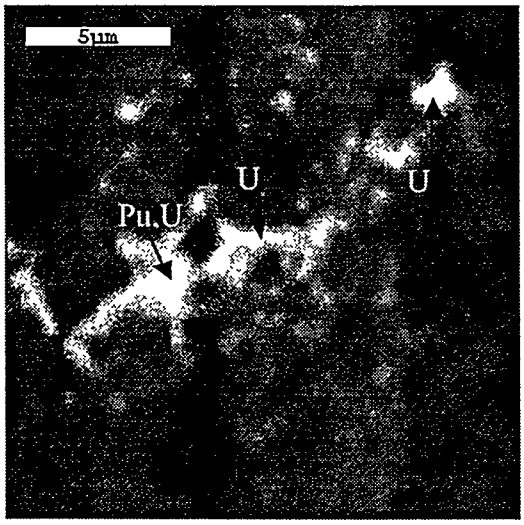

Figure 2: Scanning electron micrograph (BSE) illustrating typical actinide inclusions. Uranium containing inclusions are labeled U, while Pu,U indicates an inclusion containing both uranium and plutonium.

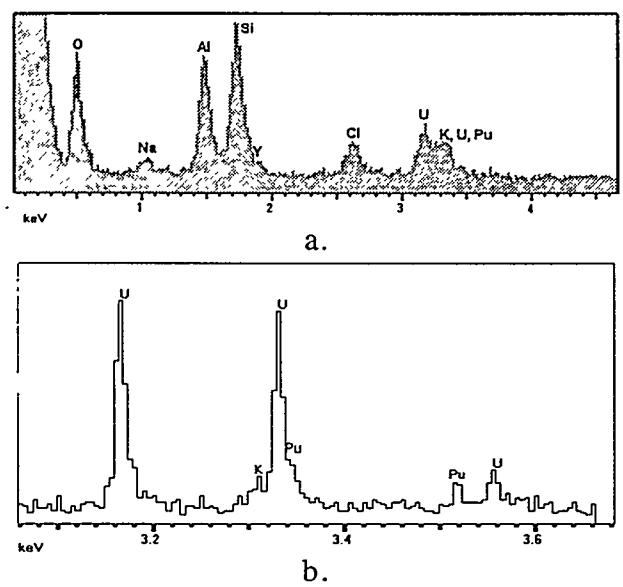

Figure 3: a. EDS and b. WDS spectra from the inclusion labeled Pu,U in Fig. 2. The Pu Mα peak at 3.347 keV appears as a low shoulder on the U Mβ peak at 3.336 keV.

supporting data from X-ray powder diffraction, suggest that of the elements identified in the spectra shown in Fig. 3, only uranium, plutonium yttrium, and oxygen are likely present in the inclusion labeled Pu,U in Fig. 2. Signals from the other elements (and some of the oxygen signal as well) probably originate in neighboring (including underlying) sodalite and glass phases.

Often, the actinide bearing inclusions in the CWF appear to consist of only UO_2, or a solid solution of $(U, Pu)O_2$. The X-ray spectra shown in Fig. 3 are representative of some of the actinide bearing inclusions found in fully radioactive CWF material, except that rare earths Nd, La, and Ce are usually present in place of Y, and in higher concentrations. These tentative interpretations of X-ray spectroscopy data from the SEM are supported by rare observations of inclusions large enough to allow less ambiguous interpretation of the spectroscopy data than the more common inclusions such as those shown in Fig. 2. Clearly, however, instrumental limitations preclude unambiguous identification of actinide bearing phases in the CWF by SEM alone.

The TEM is not subject to the same instrumental limitations as the SEM. Higher resolution in the TEM allows more detailed imaging of fine features, and, while quantitative analysis of X-ray spectroscopic data is more difficult because of specimen geometry, qualitative X-ray spectroscopy coupled with electron diffraction can be used to unambiguously identify crystalline phases.

Figure 4 is a TEM image of a representative region of CWF material. Comparing Figs. 1a and 2 to Fig. 4, the bright actinide rich strands and inclusions in the SEM images are resolved as fine crystals or very fine nanocrystals of actinide oxides in Fig. 4.

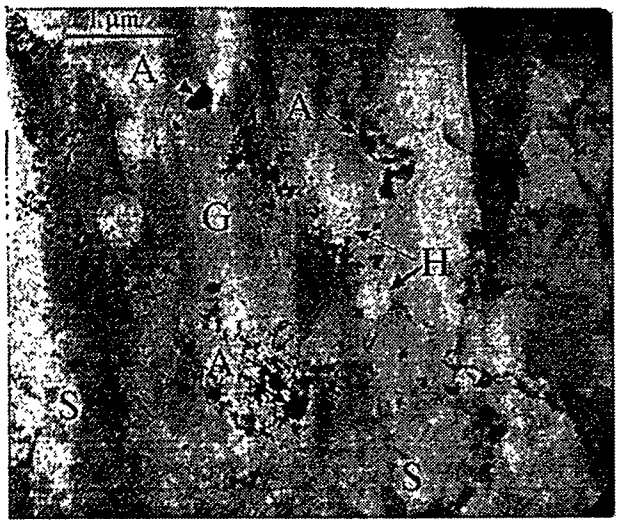

Figure 4: Bright field TEM image of a representative region of CWF material. S = sodalite, G = glass, H = halite, and A = "larger" actinide oxide crystals. The very fine dark specks are actinide oxide nanocrystals.

Figure 5a shows a higher magnification image of a cluster of (U, Pu)O_2 crystals surrounded by glass, and the corresponding EDS spectrum from this cluster (Fig. 5b). The relative intensities of the uranium and plutonium Lα lines indicate that uranium is the predominant actinide species in this cluster of crystals. The electron diffraction pattern in Fig. 5c shows an excellent match to the calculated cubic (fluorite structure) UO_2 pattern. The crystal structure data from the electron diffraction pattern allows the Si, Al, and Na peaks in the EDS spectrum in Fig. 5b to be unambiguously assigned to the glass matrix. Compared to the EDS spectrum in Fig. 3a, the spectrum in Fig. 5b shows no Cl line, and the Al line is considerably weaker. This is because the EDS spectrum from the TEM is generated from a much smaller sample volume that contains only glass and the (U,Pu)O_2 mixed oxide phase. Electron diffraction data further identify this phase as having the expected cubic (fluorite) structure.

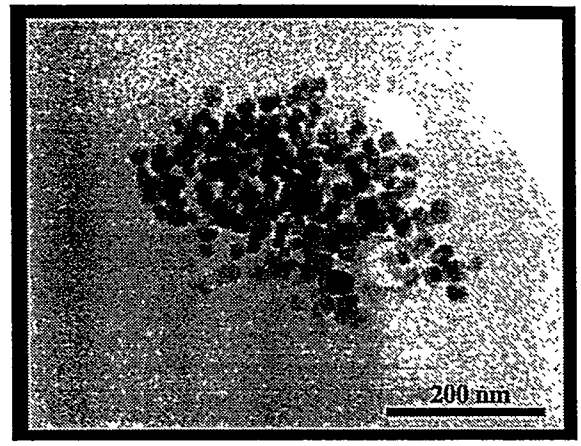

a.

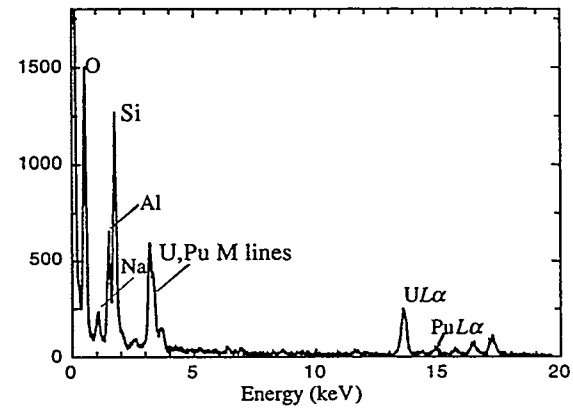

b.

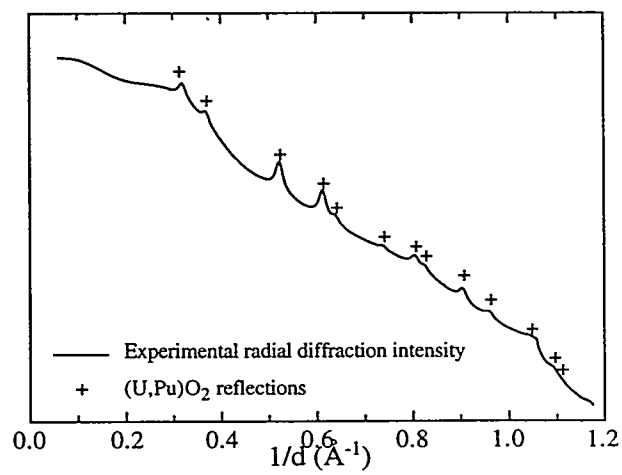

c.

Figure 5: a. Bright field TEM image of a cluster of (U,Pu)O_2 nanocrystals surrounded by glass. Note the spherical halite crystal in the lower right hand portion of the cluster. b. EDS spectrum from the cluster in a. c. Circumferentially averaged electron diffraction ring pattern from the cluster in a.

An orthorhombic rare earth silicate phase has also been identified as a minor actinide host in the CWF. While electron diffraction patterns from this phase have not been matched to any known rare earth silicate phase, the lattice parameters of the orthorhombic unit cell have been measured as: a = 22.9Å, b = 9.9Å, and c = 7.2Å. Rare earths are introduced into the CWF as fission products from the electrorefiner salt. Rare earth chlorides are converted to oxides and/or oxychlorides during the contacting step when salts are absorbed by the zeolite, and are converted to silicates during the consolidation step in the HIP. The rare earth silicate phase appears to show a preferential solubility for plutonium. Figure 6 shows a TEM image of typical rare earth silicate crystals, along with an EDS spectrum and an electron diffraction pattern. The nearly equal intensities of the U and Pu Lα lines in the spectrum of Fig. 6b (at 13.62 and 14.62 keV respectively) indicate roughly equal concentrations of uranium and plutonium in the rare earth silicate phase. This suggests a preferential solubility for plutonium as compared to the spectrum from the (U, Pu)O_2 solid solution phase where the relative concentration of Pu is lower as shown in the spectrum in Fig. 5b. The spectrum in Fig. 5b is more typical of what would be expected from the relative ratio of uranium to plutonium in the starting salt mixture (see Table 1).

The occurrence of actinides and rare earths as oxides and silicates was unexpected, as these elements are present in the electrorefiner salt as chloride species. It was originally assumed that all the chloride species would be occluded into the zeolite structure and retained in the sodalite. The first indication that this assumption might not be entirely correct came during development work with non-radioactive materials, when small, rare earth rich phases were observed in CWF samples. EDS spectra from the SEM indicated that these phases were either oxides or silicates, but because of the small size of these phases positive identification was impossible. SEM examination of the salt occluded zeolite starting material revealed small rare earth deposits on the surfaces of the zeolite granules. EDS spectra indicated the deposits were either oxides or oxychlorides, but again the small size of the deposits prevented positive identification.

a.

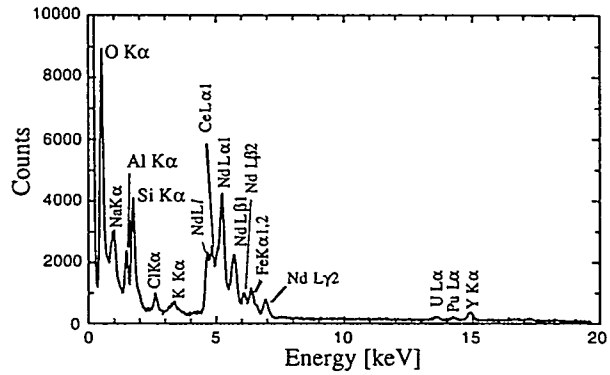

b.

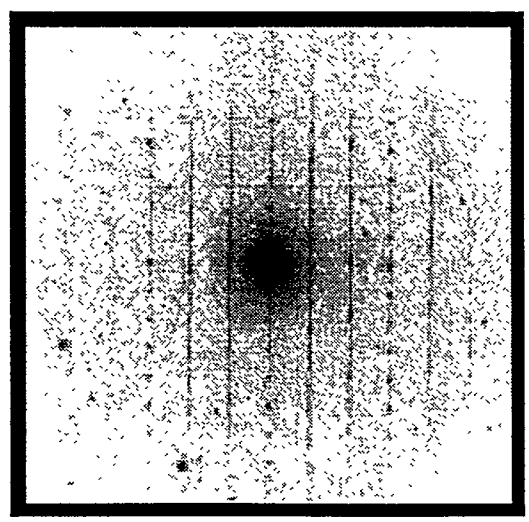

c.

Figure 6: a. Bright field TEM image showing actinide bearing rare earth silicate crystals (R). The fine dark objects in the image are (U, Pu)O_2 nanocrystals. b. EDS spectrum from one of the rare earth silicate crystals in a. c. Electron

diffraction pattern ([010] zone axis) from a rare earth silicate crystal in a. Vertical streaking in the pattern indicates the presence of stacking disorder.

Thermodynamic calculations confirmed that at the temperature at which the salt absorption step is performed rare earth oxychloride formation is possible by reaction with residual water in the zeolite. Conversion of rare earth oxychlorides to silicates takes place during the consolidation step in the HIP, probably involving reaction with the glass phase as the source of silica. Yttrium was found to behave like the rare earths with respect to these reactions. Later, it was found that uranium and plutonium behave similarly, except that these form oxides during the absorption step instead of oxychlorides. These reactions offer a plausible explanation for the occurrence of rare earth silicate and (U, Pu)O_2 crystals in the CWF. Other fission products have never been observed during microscopic examination of non-radioactive (made with surrogate fission products) or fully radioactive CWF samples. Presumably, this is because they are distributed throughout the sodalite phase (or perhaps the sodalite and glass phases), so that their concentrations are below detectability limits.

Another unexpected feature of CWF material is the presence of halite crystals, which usually occur in the glass phase, but near glass/sodalite interfaces. A possible explanation for the formation of halite crystals is suggested by the TEM image in Fig. 7. A particularly dense area of halite crystals is shown near a glass/sodalite interface, with a rough line of (U, Pu)O_2 nanocrystals apparently displaced into the glass. Recalling that the (U, Pu)O_2 crystals were originally on the surface of the zeolite, this image suggests that some of the halide bearing aluminosilicate (zeolite or sodalite) may have been dissolved by the glass during consolidation at high temperature in the HIP, leaving the (U, Pu)O_2 crystals behind. Halite crystals are precipitated in place because of the low solubility of chlorine in the glass.

This hypothesis is supported by X-ray spectroscopy data collected by operating the SEM in line scan mode. Figure 8a shows a SEM image of a glass inclusion in a sample of non-radioactive CWF material. The nearly vertical line in the image shows where the electron beam was repeatedly rastered to collect EDS data.

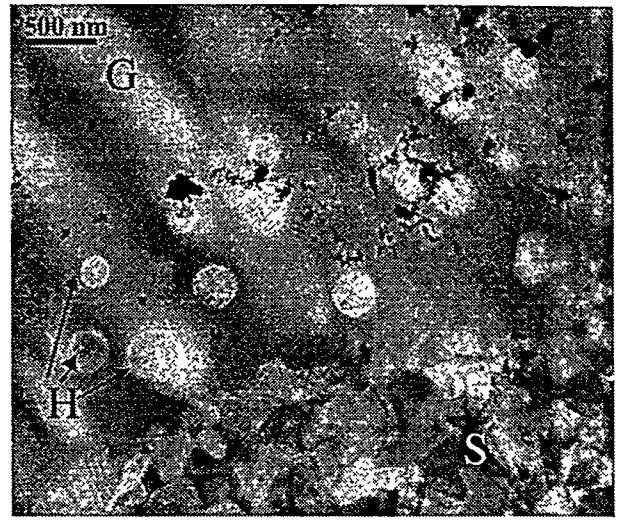

Figure 7: Bright field TEM image of the glass/sodalite interface region. G = glass, H = halite, S = sodalite. The small dark objects are (U, Pu)O_2 crystals.

Figure 8b shows the aluminum concentration along this line. Clearly, a concentration gradient extends into the glass from the glass/sodalite interface. The observed gradient, which extends over tens of microns, cannot be attributed to systematic effects such as beam spreading, which produces an activation volume only about 2 μm in diameter. The gradient appears to approximate an exponential curve, suggesting non-steady state diffusion of aluminum into the glass behind the dissolution front. The aluminum concentration in the center portion of the glass inclusion (about 40 μm to 120 μm from the origin of the line, indicated by the circled plus sign) averages 3.2 at%. This compares to 2.4 at% (adjusted to discount the presence of boron, which cannot be detected in this matrix by X-ray spectroscopy) measured on the starting material (glass additive) by wet chemical analysis. A significant decrease in sodium and increase in potassium in the glass in the CWF material compared to the composition of the starting material suggests the possibility of an ion exchange reaction between the glass and the aluminosilicate (zeolite or sodalite) during the high temperature consolidation step. This reaction may include migration of lithium (which

cannot be detected by X-ray spectroscopy) from the aluminosilicate into the glass. The presence of undetected elements such as lithium would bias measured concentrations of other elements towards higher values. Thus, the measured concentration of aluminum near the center of the glass inclusion shown in Fig. 8a compares reasonably well with the concentration measured on the starting material by wet chemical analysis. Satisfactory agreement (within experimental uncertainty) of the aluminum concentration near the center of the inclusion measured by X-ray spectroscopy and the aluminum concentration in the starting material measured independently supports the hypothesis that the observed concentration gradients result from a non-steady state diffusion process that was arrested by termination of the HIP cycle.

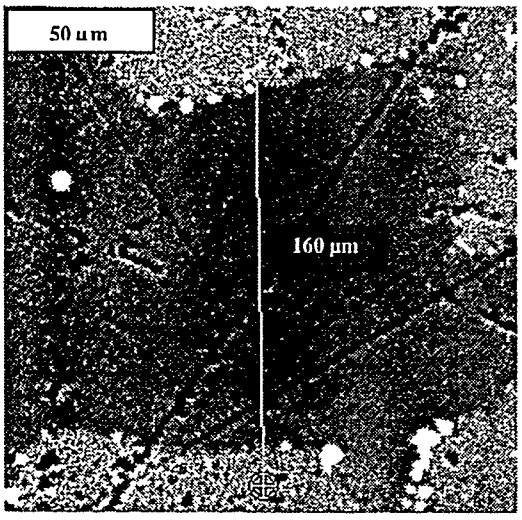

a.

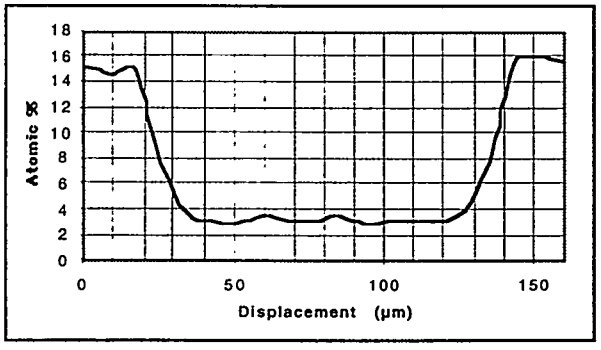

b.

Figure 8: a. Back scattered electron micrograph of a glass inclusion surrounded by sodalite. The line shows the position of the line scan from which EDS spectroscopy data was collected. The micrograph's size bar is in the upper left hand corner, while the number next the line indicates the length of the line. The electron beam was rastered from the bottom of the line to the top to collect the X-ray data. Bright white spots in the image are halite crystals. b. Concentration data as a function of position along the line in a. derived from the Al Kα characteristic X-ray line.

IV. CONCLUSIONS

The microstructure of the CWF consists primarily of sodalite granules bonded together with intergranular glass. Rare earth (and yttrium) fission products and actinides are present as separate crystalline phases because of reactions that occur during the salt absorption step and/or the consolidation step in the HIP. Other fission products are present in concentrations too low to be detected, presumably indicating that they are distributed throughout the sodalite phase. The presence of halite crystals in the glass near glass/sodalite interfaces, along with X-ray spectroscopy data, suggests that some of the aluminosilicate phase (as zeolite or sodalite) is dissolved by the glass during consolidation in the HIP.

ACKNOWLEDGMENTS

This work was supported by the Department of Energy, Nuclear Energy Research and Development Program, under contract No. W-31-109-ENG-38. The authors thank M. Simpson, K. Bateman, and the staff of the Hot Fuel Examination Facility for producing the waste forms.

REFERENCES

1. Ceramic Waste Form Handbook, compiled by L. R. Morss, ANL-NT-119, available from Argonne National Laboratory, Argonne, IL 60439 (1999).